Proc. Natl. Acad. Sci. USA
Vol. 87, pp. 8541–8544, November 1990
Chemistry

Direct structure analysis of a paraffin solid solution

(electron diffraction/electron microscopy/direct phase determination/binary organic solids/epitaxial orientation)

DOUGLAS L. DORSET

Electron Diffraction Department, Medical Foundation of Buffalo, 73 High Street, Buffalo, NY 14203

Communicated by Herbert A. Hauptman, August 10, 1990 (received for review May 10, 1990)

ABSTRACT **Single microcrystals of a 1:1 solid solution of n-$C_{32}H_{66}$/n-$C_{36}H_{74}$ have been grown by epitaxial nucleation on benzoic acid, and 0*kl* electron diffraction patterns from them can be obtained with a lamellar spacing characteristic of the intermediate n-paraffin n-$C_{34}H_{70}$. This average structure is also indicated by indices (space group $Pca2_1$) for major intensities in this zone. Direct phasing of the intensity data is carried out by combined use of low-dose electron microscope lattice images (to assign values to the "lamellar" reflections) and three-phase structure invariant relationships (to find values for the "polyethylene" reflections). The computed electrostatic potential map closely resembles the crystal structure of n-$C_{34}H_{74}$, for which all 34 atom positions can be found. It is apparent, however, that lower atomic occupancies at the chain ends correspond to anticipated disorder at the lamellar interface. Structural refinement based on this occupancy results in a good match to the observed intensity data.**

Binary solids of n-alkane chains serve as an important model for numerous polydisperse linear molecules—from lipids to polyethylene. Although, historically, numerous studies have been made of these binary combinations in an effort to understand the structural rules that determine the stable cosolubility of such molecules in the solid state [e.g., as discussed in the 1960 review by Mnyukh (1)], the recent availability of epitaxially oriented microcrystalline preparations has enabled these determinations to be made routinely in terms of a single-crystal structure (2–6). The molecular volume differences tolerated as a stable solid solution have been shown experimentally (6) to be dependent upon the mean molecular chain length, with a relationship similar to the prediction of Matheson and Smith (7). Symmetry rules, on the other hand, are somewhat different than those proposed by Kitaigorodskii (8) so that, for two pure paraffins with the same crystal structure, a stable solid solution need not crystallize with the same space group symmetry (4).

To determine the crystal structures of paraffin solid solutions, powder x-ray data have been most often employed. Kitaigorodskii *et al.* (9), in an attempt to explain the observed deviation of intermediate solid solution lamellar spacings from the linear relationship predicted by Vegard's law (1), had proposed that the crystal lattice of the longer chain component dominates solutions containing large amounts of this species. Powder x-ray diffraction lamellar intensities were found to have a rather sharp falloff compared to those from pure components, and, within the structural framework proposed by Kitaigorodskii *et al.* (9), the longitudinal translational slip of the shorter component was found to account best for these diffraction data (10). A similar conclusion was reached by Craievich *et al.* (11), although these authors described an odd–even chain combination in a solid solution, which might have been thought to be unstable, based upon Kitaigorodskii's symmetry criteria (8). A qualitative single x-ray crystal structure analysis, carried out by Lüth *et al.* (12) for an n-eicosane/n-docosane solid solution, demonstrated the same sort of atomic occupancy falloff for the outer carbon atoms in a lamellar layer. Again Kitaigorodskii's symmetry rules were violated, since many of the solid solutions were shown to have a unit cell with higher (orthorhombic) symmetry than that of the pure components (triclinic).

My first attempt to determine the structure of a solid solution quantitatively with single-crystal diffraction data was carried out with electron diffraction intensities from a 1:1 solution of n-dotriacontane/n-hexatriacontane (2). A model with fractional chain end atomic occupancies was also found to fit the observed data reasonably well (2). Although the indices of major 0*kl* reflections corresponded to the crystal structure of n-$C_{34}H_{70}$, the continuous scattering from a model based on the unit cell of n-$C_{36}H_{74}$ was sampled at reciprocal lattice positions corresponding to the C_{34} alkane, thus incorporating some features of the longer alkane transform into the structural model.

It is apparent that, when only a few number of data are recorded, the precision of the crystallographic residual for determining the best structural model is rather limited (13), given that the number of variable parameters is relatively large. To overcome this limitation, I report a determination of this structure, employing direct phasing methods based on the combination of high-resolution electron microscopy with triplet structure invariant relationships.

MATERIALS AND METHODS

Electron Microscopy and Diffraction. As described in an earlier paper (2), electron diffraction patterns (Fig. 1 *Upper*) were recorded on Kodak DEF-5 x-ray film from microcrystals of n-$C_{32}H_{66}$/n-$C_{36}H_{74}$ that had been epitaxially nucleated on benzoic acid following the procedure of Wittman *et al.* (14), within the concentration limits of the quasi-binary phase diagram of the paraffin mixture with the carboxylic acid (15). The molar ratio of the two components is near 1:1 and will be identified as such in this paper, although $x_{C36} = 0.47$. The electron microscope used was a JEOL JEM-100B7 operating at 100 kV, taking usual precautions that the radiation exposure to the specimen was kept to a minimum (16). Electron diffraction intensity data were obtained by scanning the films with a Joyce–Loebl MkIIIC flat-bed microdensitometer and then integrating under the peaks using a triangular approximation. There is no Lorentz correction applied to these data.

Low-dose electron microscopy was then carried out at a direct magnification of ×17,000 with the same preparation and the same instrument. The procedure for this microscopy has been reported (3). Suitably crystalline areas (Fig. 1 *Lower*) were identified by scanning the experimental micrographs on a laser-illuminated optical bench. These areas were then converted to a digitized image file by densitometry of the film with an Optronics P-1000 rotating drum instrument. By using the software in the image processing package IMAGIC (17), the amplitudes and phases representing the Fourier

The publication costs of this article were defrayed in part by page charge payment. This article must therefore be hereby marked "*advertisement*" in accordance with 18 U.S.C. §1734 solely to indicate this fact.

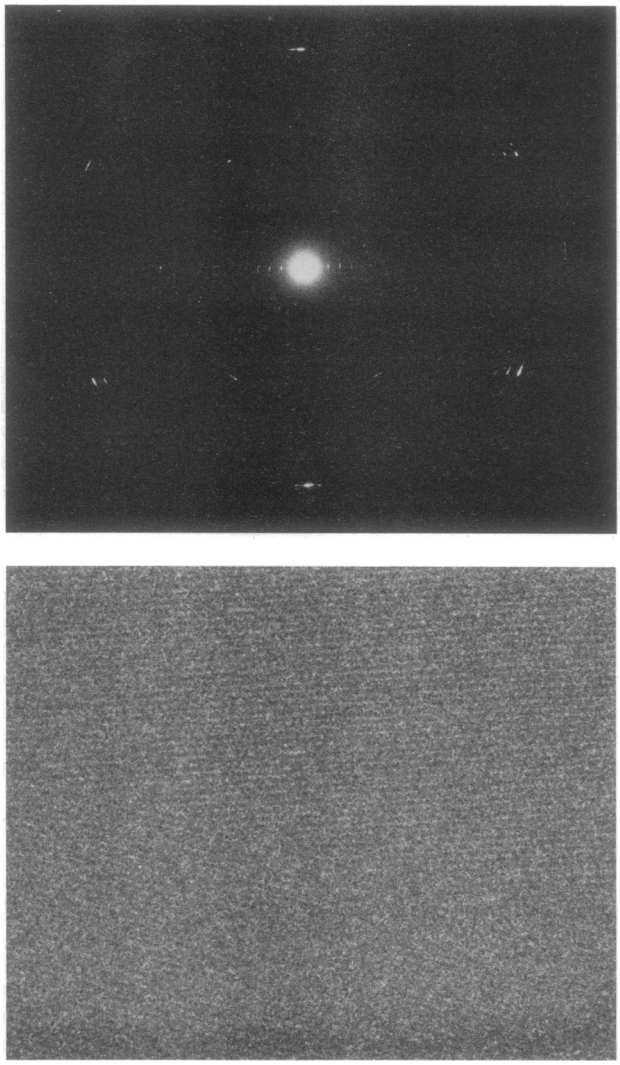

FIG. 1. (*Upper*) Electron diffraction pattern from an epitaxially crystallized 1:1 solid solution of n-$C_{32}H_{66}/n$-$C_{36}H_{74}$. The lamellar reflections near the origin are attenuated in comparison with the similar pattern from a pure paraffin. In space group $Pca2_1$, indices of the most intense polyethylene reflections are simply related to the average carbon number m of the crystal structure of an n-paraffin C_mH_{2m+2}. That is, for the $01l$ reflections, the strongest intensities are found at $l = m$ and $m + 2$, and for the $00l$ row the strongest spots (not shown) are at $l = 2m + 2$ and $2m + 4$. (*Lower*) Electron microscope lattice image of the solid solution. Computed Fourier transforms of this image allow one to determine the phases of the first two $00l$ reflections.

transform of the "lattice image" can be computed, and, when the image origin corresponds to an allowed unit cell origin, as determined by an appropriate image shift function, the phases can be used for structure analysis. (Sources of phase error, due to a dynamical scattering, are minimized by the small crystal thickness and low atomic number of the scattering species.) For the phase determination, a subarea of Fig. 1 *Lower* with a constant lamellar orientation was used for the Fourier peak filtration. For the imaging experiments carried out here, the Fourier transform peaks occur within the first envelope of the phase-contrast transfer function (18) so that they are band-passed with the same contrast sign.

Direct Phasing. Experimental structure factor magnitudes $|F_\mathbf{h}|$ were normalized to $|E_\mathbf{h}|$ using the formula

$$E_\mathbf{h}^2 = |F_\mathbf{h}|^2/\varepsilon\sum_{i=1}^{N} f_i^2,$$

where f_i is the atomic scattering factor value for atom i at (sin $\theta/\lambda)_\mathbf{h}$ and ε is a multiplicity factor to account for translational symmetry elements. Given these values, the three phase structure invariant relationships (19) among the reciprocal lattice vectors $\mathbf{h}$ can be formed—i.e.,

$$\psi = \phi_{\mathbf{h}_1} + \phi_{\mathbf{h}_2} + \phi_{\mathbf{h}_3}$$

subject to the constraint

$$\mathbf{h}_1 + \mathbf{h}_2 + \mathbf{h}_3 = 0.$$

When the reciprocal lattice vectors are all different, this is termed a sigma 2 (Σ_2) triple; when $\mathbf{h}_1 = \mathbf{h}_2$ and $\mathbf{h}_3 = -2\mathbf{h}_1$, it is termed a sigma 1 (Σ_1) triple. In the former case, the probability of the value of $\psi \simeq 0$ is assessed according to the magnitude of

$$A_2 = (2\sigma_3/\sigma_2^{3/2})|E_{\mathbf{h}_1}E_{\mathbf{h}_2}E_{\mathbf{h}_3}|,$$

where

$$\sigma_n = \sum_{j=1}^{N} Z_j^n.$$

Here, $Z_j = f_j$ at (sin θ/λ) = 0 and N is the number of atoms in the unit cell. A probability estimate of the Σ_1 triple is based on

$$A_1 = (|E_\mathbf{h}|^2 - 1)\ (|E_{2\mathbf{h}}|)/\sqrt{N}.$$

Although most of the phase determinations will be made within the symmetry operations for the noncentrosymmetric space group $Pca2_1$ (20), it has been found that certain triplet relationships can be used for lamellar reflections, partcularly when two domains with large intensity are separated in the reciprocal row by a low-intensity node. Since the row is pseudocentrosymmetric (because the molecules themselves have centrosymmetry), we can halve the Miller indices for this analysis to assume that the scattering is from an array of single lamella in space group $P\bar{1}$.

RESULTS

Although it is also possible to find microcrystals of a 1:1 solid solution of n-$C_{32}H_{66}/n$-$C_{36}H_{74}$ that diffract as if they were pure n-$C_{35}H_{72}$ in space group $A2_1am$ (4), we have used examples that crystallize in the same orthorhombic space group, $Pca2_1$, as do the two pure components. (For the $0kl$ data considered here, the latter space group is identified by the extinct reflections occurring at $l = 2n + 1$.) The unit cell constants used for structure factor calculations are based on the parameters expected (21) for the paraffin n-$C_{34}H_{70}$ (i.e., a = 7.42, b = 4.96, and c = 90.05 Å). Values of a and b measured from $hk0$ electron diffraction patterns are close to these axial distances with a measured standard deviation of ±1%. For the long axis, the measured value is slightly higher, with $c/2$ = 45.77 ± 0.67 Å, using patterns that index as n-$C_{34}H_{70}$. As shown in Fig. 1 *Upper*, the $0kl$ electron diffraction pattern resembles that of a pure even-chain n-paraffin (22) except that the resolution of the inner $00l$ reflections is greatly reduced.

The sequence of direct phase determination for a 1:1 solid solution of n-$C_{32}H_{66}/n$-$C_{36}H_{74}$ is outlined below.

Electron microscopy: $\phi_{002} = \phi_{004} = \pi$
Three-phase structure invariants:
  $0kl$ reflections
    Σ_1 triples: numerous indications that $\phi_{020} = \pi$
    Σ_2 triples: origin definition $\phi_{0,3,36} = \pi/2$
      $\phi_{0,0,70} = a$

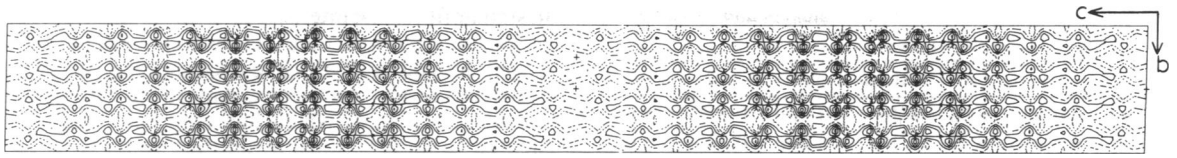

FIG. 2. Electrostatic potential map computed from the phased structure factors (see Table 1). The [100] projection is very similar to the structure of a pure paraffin except that the atomic occupancies deviate from the atomic occupancy value $p = 1.0$ toward the chain ends.

$\phi_{0,0,72} = \pi$
$\phi_{0,1,34} = \pi/2$
$\phi_{0,1,36} = -\pi/2$
$\phi_{0,2,70} = a + \pi$
$\phi_{0,2,72} = 0$
$\phi_{0,3,34} = -\pi/2$

00l reflections (pseudo $P\bar{1}$)
Σ_1 triples: $\phi_{004} = \phi_{008} = \pi$
Σ_2 triples: $\phi_{0,0,70} = 0 = a$

As will be shown elsewhere for electron diffraction data from a pure n-paraffin, the Σ_2 triples allow the phases of most intense "polyethylene" reflections in the 0kl diffraction pattern to be determined. Since numerous Σ_1 triples indicate that $\phi_{020} = \pi$, one of the two possible phases for origin definition allowed in the zone (i.e., $\phi_{0,3,36} \simeq \pi/2$) can be defined *a priori* so that the simultaneous equations in Σ_2 triples can be used to find the values of other phases. These relationships are found to be valid for $A_2 \geq 0.2$.

It is noted that there are no Σ_2 relationships between low-angle 00l reflections and the intense 0kl reflections that have an A_2 value high enough to be useful. By using only the lamellar data and combining the electron microscopy data with the direct phasing of the 0kl reflections, it can be shown that if $\phi_{002} = \pi$ and $\phi_{0,0,72} = \pi$, then $\phi_{0,0,70} = 0$ from a Σ_2 triplet. Σ_1 triplets indicate also that $\phi_{0,0,8} = \pi$. Comparing these phase values to those obtained from structural models based on pure n-$C_{34}H_{70}$ or a disordered n-$C_{36}H_{74}$ model (2), it is found that the best agreement points to the pure paraffin model in that the actual phases are closest to centrosymmetric values.

Of all of the most intense diffraction data, 12 out of 20 reflections have been assigned phase values by the combination of electron microscopy and triple structure invariant relationships. (Thus the phases of 8 major reflections remain undefined.) An electrostatic potential map calculated from the 12 phased observed structure factors (Fig. 2) clearly indicates the positions of all 34 chain atoms in the expected chain packing motif for the [100] projection of n-$C_{34}H_{70}$ in $Pca2_1$. From the contour levels of these atoms, however, it is clear that the major packing density is located in the chain centers and that the atomic occupancy decreases toward the chain ends. A one-dimensional electrostatic potential map, calculated with the 00l reflections only, can be used to determine the falloff of the atomic occupancy (Fig. 3) more clearly than in the two-dimensional map.

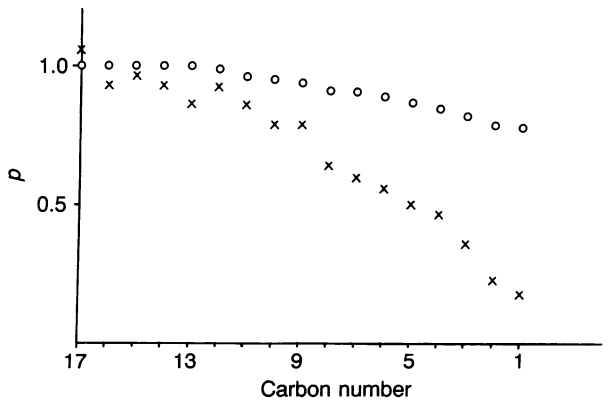

FIG. 3. Carbon atom occupancy values p indicated by the map in Fig. 2. The values obtained directly from the reverse Fourier transform (×) do not provide a good match to the observed intensity data. When the values $1.0 - p$ are multiplied by 1/4 (○), the fit is much better.

If the chain carbon positions are used to calculate structure factors using the atomic occupancies p suggested by the Fourier map (Fig. 3), the match to the observed data is rather poor ($R = 0.52$). The falloff of chain atom occupancy factors, therefore, is somewhat exaggerated in the calculated maps. Weighting the occupancy difference $(1.0 - p)$ by 1/4 results in a better match to the observed data ($R = 0.29$). A final structure factor calculation including hydrogen atom positions, assuming tetrahedral geometry, lowers the crystallographic residual to $R = 0.23$, as shown in Table 1. The carbon atom positions for this structure in the projection down [100] are given in Table 2 along with their final occupancies.

DISCUSSION

The structure analysis outlined above illustrates how direct phasing techniques may be adapted to analyze crystal structures for which they are generally unsuited, given the dominance of the diffraction pattern by the strongly scattering sublattice (the so-called "methylene subcell"). If an independent source of phase information can be employed, as in the case of the electron microscopic information used in this study, to assign values to the lamellar reflections, then separately analyzed regions of the diffraction pattern can be recombined to determine the complete crystal structure. Even though phase values were assigned to only part of the

Table 1. Comparison of calculated (calc) and observed (obs) structure factors

$h\ k\ l$	$\lvert F_{obs}\rvert$	$\lvert F_{calc}\rvert$	ϕ_{calc}, °	ϕ (direct methods)
0 0 2	0.67	0.85	180.16	π
0 0 4	0.55	0.38	180.23	π
0 0 6	0.37	0.30	180.32	
0 0 8	0.27	0.30	180.73	π
0 0 68	0.27	0.26	4.30	
0 0 70	0.86	1.14	4.87	0
0 0 72	0.83	0.84	185.03	π
0 0 74	0.21	0.24	184.74	
0 1 30	0.25	0.24	93.69	
0 1 32	0.42	0.33	94.06	
0 1 34	0.81	0.90	91.65	$\pi/2$
0 1 36	1.57	1.77	−87.34	$-\pi/2$
0 1 38	0.37	0.23	−90.83	
0 2 0	1.93	2.42	180.00	π
0 2 2	0.44	0.21	−10.50	
0 2 70	0.47	0.41	185.45	π
0 2 72	0.51	0.31	4.12	0
0 3 32	0.37	0.20	−90.83	
0 3 34	0.60	0.53	−86.48	$-\pi/2$
0 3 36	1.17	1.06	92.75	$\pi/2$

Carbon positions indicated by Fig. 2 were corrected for regular chain zigzag geometry. Hydrogen atoms were generated assuming tetrahedral geometry. $B_C = 3.0$ Å^2; $B_H = 4.0$ Å^2. $R = (\Sigma\|F_{obs}| - k|F_{calc}\|)/\Sigma|F_{obs}| = 0.23$ where $\Sigma|F_{obs}| = k\Sigma|F_{calc}|$.

Table 2. Final carbon atom fractional coordinates and occupancies (p) for a 1:1 solid solution of C_{32}/C_{36}

Atom	y/b	z/c	p	Atom	y/b	z/c	p
C1	0.186	0.0173	0.78	C18	0.314	0.2572	1.00
C2	0.314	0.0314	0.79	C19	0.186	0.2714	1.00
C3	0.186	0.0455	0.82	C20	0.314	0.2855	1.00
C4	0.314	0.0596	0.85	C21	0.186	0.2996	1.00
C5	0.186	0.0738	0.87	C22	0.314	0.3137	1.00
C6	0.314	0.0879	0.89	C23	0.186	0.3278	0.99
C7	0.186	0.1020	0.91	C24	0.314	0.3419	0.96
C8	0.314	0.1161	0.91	C25	0.186	0.3560	0.95
C9	0.186	0.1302	0.94	C26	0.314	0.3702	0.94
C10	0.314	0.1443	0.95	C27	0.186	0.3843	0.91
C11	0.186	0.1584	0.96	C28	0.314	0.3984	0.91
C12	0.314	0.1726	0.99	C29	0.186	0.4125	0.89
C13	0.186	0.1867	1.00	C30	0.314	0.4266	0.87
C14	0.314	0.2009	1.00	C31	0.186	0.4407	0.85
C15	0.186	0.2149	1.00	C32	0.314	0.4548	0.82
C16	0.314	0.2290	1.00	C33	0.186	0.4690	0.79
C17	0.186	0.2431	1.00	C34	0.314	0.4831	0.78

observed diffraction pattern, the information provided is complete enough (i.e., the major features of the unit cell transform is phased) to give an interpretable map after the reverse Fourier transform is calculated.

Consistent with our earlier finding that the unit cell of a solid solution has a long axial dimension very close to that of the pure paraffin, we find from the map in Fig. 2 that the electrostatic potential distribution of a 1:1 solid solution of n-$C_{32}H_{66}/n$-$C_{36}H_{74}$ resembles the structure expected for n-$C_{34}H_{70}$ (i.e., the intermediate alkane structure). The lamellar thickness limit, therefore, is not determined by the length of the longest paraffin, as suggested in earlier model studies (1, 2). From the distribution of chain carbon occupancies, it is apparent that some random translational displacement of the shorter chain component must take place in order to minimize the volume occupied by voids in a lamella, as stated previously by Asbach *et al.* (10). On the other hand, it is also clear that some chain "kink" defects must also be present to shorten the n-$C_{36}H_{74}$ component so that it can fit within the lamellar thickness. Earlier, a model was proposed where this defect content was distributed uniformly across the chain (4) and it was found that, when a threshold limit of 2% defect content per single bond would be reached, a unit cell with the next largest average alkane chain length (odd or even) would be favored. Vibrational spectroscopic measurements (23, 24) indicate, on the other hand, that the chain disorder is not uniformly distributed along the chain but is concentrated near the chain ends. The location of the chain kinks near the lamellar interfaces would thus serve to help fill the voids produced by comixing two different chain lengths in a single lamella.

It is not possible, however, to propose an exact packing model for the solid solution crystal structure from the Bragg intensities alone. The two different models already considered in our electron diffraction studies (see also ref. 2) result in similar fits to the intensity data, although the direct phasing procedure described here clearly favors a lamellar model with a well-defined layer thickness containing partial atomic occupancies at the chain ends. Any further information about the defect content, which has only been qualitatively considered so far (25), must await the completion of a quantitative analysis of the continuous diffuse scattering.

It will be informative to apply this direct phasing analysis to diffraction patterns from a series of solid solutions with binary compositions sampling various regions of the phase diagram. In this way, the relative concentrations of chain end voids can be determined, as well as the relative packing densities for the various alternative local crystal structures observed at a given molar ratio.

This research was supported by a grant from the National Science Foundation (DMR86-10783).

1. Mnyukh, Yu, V. (1960) *Zh. Strukt. Khim.* **1,** 370–388.
2. Dorset, D. L. (1985) *Macromolecules* **18,** 2158–2163.
3. Dorset, D. L. (1986) *Macromolecules* **19,** 2965–2973.
4. Dorset, D. L. (1987) *Macromolecules* **20,** 2782–2788.
5. Zhang, W. P. & Dorset, D. L. (1990) *J. Polym. Sci. B Polym. Phys.* **28,** 1223–1232.
6. Dorset, D. L. (1990) *Macromolecules* **23,** 623–633.
7. Matheson, R. R., Jr., & Smith, P. (1985) *Polymer* **26,** 288–292.
8. Kitaigorodskii, A. I. (1961) *Organic Chemical Crystallography* (Consultant's Bureau, New York), pp. 231–240.
9. Kitaigorodskii, A. I., Mnyukh, Yu, V. & Nechitailo, N. A. (1958) *Sov. Phys. Crystallogr.* **1,** 303–307.
10. Asbach, G. I., Geiger, K. & Wilke, W. (1979) *Colloid Polym. Sci.* **257,** 1049–1059.
11. Craievich, A., Doucet, J. & Denicolo, J. (1984) *J. Phys. (Paris)* **45,** 1473–1477.
12. Lüth, H., Nyburg, S. C., Robinson, P. M. & Scott, H. G. (1974) *Mol. Cryst. Liq. Cryst.* **27,** 337–357.
13. Hamilton, W. C. (1964) *Statistics in Physical Science: Estimation, Hypothesis Testing and Least-Squares* (Ronald, New York), pp. 157–162.
14. Wittmann, J. C., Hodge, A. M. & Lotz, B. (1983) *J. Polym. Sci. Polym. Phys. Ed.* **21,** 2495–2509.
15. Dorset, D. L., Hanlon, J. & Karet, G. (1989) *Macromolecules* **22,** 2169–2176.
16. Dorset, D. L. (1985) *J. Electron Microsc. Techn.* **2,** 89–128.
17. Heel, M. v. & Keegstra, W. (1981) *Ultramicroscopy* **7,** 113–130.
18. Erickson, H. P. (1973) *Adv. Optical Electron Microsc.* **5,** 163–199.
19. Hauptman, H. A. (1972) *Crystal Structure Determination: The Role of the Cosine Seminvariants* (Plenum, New York).
20. Henry, N. F. M. & Lonsdale, K., eds. (1969) *International Tables for X-ray Crystallography* (Kynoch, Birmingham, U.K.), Vol. 1, 3rd Ed.
21. Nyburg, S. C. & Potworowski, J. A. (1973) *Acta Crystallogr. B* **29,** 347–352.
22. Moss, B., Dorset, D. L., Wittmann, J. C. & Lotz, B. (1984) *J. Polym. Sci. Polym. Phys. Ed.* **22,** 1919–1929.
23. Maroncelli, M., Strauss, H. L. & Snyder, R. G. (1985) *J. Phys. Chem.* **89,** 5260–5257.
24. Kim, Y., Strauss, H. L. & Snyder, R. G. (1989) *J. Phys. Chem.* **93,** 485–490.
25. Dorset, D. L., Moss, B. & Zemlin, F. (1985–1986) *J. Macromol. Sci. Phys. B* **24,** 87–97.